

Numerical solution of the linearized fixed gravimetric boundary-value problem

R. Čunderlík · K. Mikula · M. Mojzeš

Received: 4 May 2006 / Accepted: 19 March 2007 / Published online: 1 May 2007
© Springer-Verlag 2007

Abstract The fixed gravimetric boundary-value problem (FGBVP) represents an exterior oblique derivative problem for the Laplace equation. Terrestrial gravimetric measurements located by precise satellite positioning yield oblique derivative boundary conditions in the form of surface gravity disturbances. In this paper, we discuss the boundary element method (BEM) applied to the linearized FGBVP. In spite of previous BEM approaches in geodesy, we use the so-called direct BEM formulation, where a weak formulation is derived through the method of weighted residuals. The collocation technique with linear basis functions is applied for deriving the linear system of equations from the arising boundary integral equations. The nonstationary iterative biconjugate gradient stabilized method is used to solve the large-scale linear system of equations. The standard MPI (message passing interface) subroutines are implemented in order to perform parallel computations. The proposed approach gives a numerical solution at collocation points directly on the Earth's surface (on a fixed boundary). Numerical experiments deal with (i) global gravity field modelling using synthetic data (surface gravity disturbances generated from a global geopotential model (GGM)) (ii) local gravity field modelling in Slovakia using observed gravity data. In order to

extend computations, the memory requirements are reduced using elimination of the far-zone effects by incorporating GGM or a coarse global numerical solution obtained by BEM. Statistical characteristics of residuals between numerical solutions and GGM confirm the reliability of the approach and indicate accuracy of numerical solutions for the global models. A local refinement in Slovakia results in a local (national) quasigeoid model, which when compared with GPS-levelling data, does not make a large improvement on existing remove-restore-based models.

Keywords Linearized fixed gravimetric boundary-value problem (LFGBVP) · Boundary element method (BEM) · Method of weighted residuals · Collocation · Piecewise linear basis functions · Parallel computing · Global and local gravity field modelling

1 Introduction

The determination of the Earth's external gravity field is usually formulated in terms of the geodetic boundary-value problem (BVP) for the Laplace equation. The classical approaches, e.g., the Stokes problem (Stokes 1846) or the linearized Molodenskij problem (Molodenskij et al. 1962, later extended by Krarup 1973 and Moritz 1980), involve boundary conditions (BC) in the form of the well-known fundamental equation of physical geodesy. Here the input gravity anomalies (geoidal or surface) are considered on the boundaries that only approximate the real Earth's surface, i.e., on the geoid or telluroid, respectively.

In recent decades, more attention has been focused on the fixed gravimetric BVP (FGBVP), where the physical surface of the Earth is assumed to be known. Without any doubt, the

R. Čunderlík (✉) · M. Mojzeš
Department of Theoretical Geodesy, Faculty of Civil Engineering,
Slovak University of Technology, Radlinského 11,
813 68 Bratislava, Slovakia
e-mail: cunderli@svf.stuba.sk

M. Mojzeš
e-mail: marcel.mojzes@stuba.sk

K. Mikula
Department of Mathematics and Descriptive Geometry,
Faculty of Civil Engineering, Slovak University of Technology,
Radlinského 11, 813 68 Bratislava, Slovakia
e-mail: mikula@math.sk

precise 3D positioning by GNSS (global navigation satellite systems) has brought new possibilities in gravity field modelling. Terrestrial gravimetric measurements located by precise geocentric positioning directly provide surface gravity disturbances. They almost correspond to negative values of derivatives of the unknown disturbing potential at points on the Earth's surface. It means they represent the oblique derivative BC for the linearized FGBVP. At the same time, the Earth's surface is given as a fixed boundary.

A uniqueness theorem for a non-linear FGBVP was first given by Backus (1968). The existence and uniqueness of the solution for the associated linear (or linearized) problem was introduced by Koch and Pope (1972). They also gave a uniqueness proof for the non-linear case. This general problem was later discussed by Bjerhammar and Svensson (1983), Sacerdote and Sansó (1989) and Grafarend (1989). Later on, many authors have dealt with the FGBVP (e.g., Heck 1989a,b; Holota 1997, 2005).

In this paper, we discuss a numerical solution of the linearized FGBVP, where BC are considered in the form of the surface gravity disturbances. It represents an exterior oblique derivative problem for the Laplace equation. We use the boundary element method (BEM), which is suitable for solving exterior BVPs. BEM, as a numerical method, is based on a weak formulation of a partial differential equation (PDE). Its principle consists in an approximation of the unknown quantity by a function that satisfies the PDE exactly, but the BC only approximately.

The advantage of BEM is that only the boundary of the solution domain requires a subdivision into its elements. Thus, the dimension of the problem is effectively reduced by one. The reformulation of the PDE consists of the surface integral equations defined on the boundary, i.e., on the Earth's surface. They are transformed into a linear system of equations by an appropriate numerical technique, e.g., by the collocation method or the Galerkin BEM (see, e.g., Brebbia et al. 1984; Hartmann 1989; Schwarz et al. 1990; Lucquin and Pironneau 1998). Such approach leads to a numerical solution that is as close as possible to reality, but the price to be paid is a numerical complexity.

First application of BEM to gravity field modelling was given by Klees (1992). This approach based on the Galerkin BEM was gradually extended (Klees 1998; Lehmann 1997c). In order to reduce the numerical complexity of BEM, parallel computing (Lehmann and Klees 1996; Lehmann 1997a,b) and compression techniques such as panel clustering and the fast multipole method were implemented. This effort results in very sophisticated approaches (Klees and Lehmann 2001; Klees et al. 2001). All these BEM applications use the single layer potential 'ansatz' for reformulating the Laplace equation, i.e., they are based on the indirect BEM formulation.

In our approach, we use a direct BEM formulation, where the boundary integral equations (BIEs) can be derived

through the application of Green's third identity or through the method of weighted residuals (Brebbia et al. 1984). Both methods lead to the same integral relation. In this paper, we use the weighted residuals technique, which can be understood as a weak formulation of the problem. In order to discretize BIEs and transform them into the linear system, we consider the collocation method with linear basis functions. Such approach provides a numerical solution directly at points on the Earth's surface, which is discretized into finite elements. Taking into account that the exterior BVP for the Laplace equation with the Neumann BC admits a unique solution that is regular at infinity (Brebbia et al. 1984), we will show how to project the oblique derivative BC into the Neumann BC. This step includes a simplification that is acceptable for the practical purposes and makes numerical experiments easier to implement.

The main drawback of the BEM application is its numerical complexity. The obtained system matrix is dense and non-symmetric. Therefore, enormous memory requirements are a main limitation for numerical computations. With respect to the size of the Earth and in order to get accuracy as high as possible, computing on parallel computers is inevitable. In our applications, the number of equations is more than 10^4 and can feasibly increase to 10^6 or more.

There are several options to reduce the memory requirements. An application of the linear basis functions instead of constant ones in our approach reduces the memory requirements by a factor of four (Čunderlík 2004). Recently, numerous compression techniques have been developed to reduce the numerical complexity of BEM, e.g., the fast multipole methods (Greengard and Rokhlin 1987), panel clustering (Hackbusch and Nowak 1989), wavelet techniques and others. Their implementation to the gravity field modelling by BEM is discussed in (Klees et al. 2001).

In our approach, we simply reduce memory requirements by incorporating a priori known approximate values obtained from a global geopotential model (GGM) or from numerical solutions computed on coarse grids. This permits us to transform the original dense stiffness matrix into a sparse one, allowing further computation extensions that can yield more precise numerical solutions.

2 The linearized fixed gravimetric BVP

The linearized FGBVP represents an exterior oblique derivative problem for the Laplace equation (cf. Koch and Pope 1972; Bjerhammar and Svensson 1983; Grafarend 1989). Following the definition of the disturbing potential T ,

$$T(\mathbf{x}) = W(\mathbf{x}) - U(\mathbf{x}), \quad \mathbf{x} \in R^3, \quad (1)$$

where W is the actual and U the normal gravity potential at any point \mathbf{x} and according to assumptions for the same

problem described in Holota (1997), the problem may be formulated as:

$$\Delta T(\mathbf{x}) = 0, \quad \mathbf{x} \in R^3 - \Omega, \tag{2}$$

$$\langle \nabla T(\mathbf{x}), \mathbf{s}(\mathbf{x}) \rangle = -\delta g(\mathbf{x}), \quad \mathbf{x} \in \Gamma, \tag{3}$$

where the domain Ω is the body of the Earth with its boundary Γ (the Earth's surface), $\langle \cdot, \cdot \rangle$ represents the inner product of vectors, ∇ is the gradient operator and

$$\mathbf{s}(\mathbf{x}) = -\nabla U(\mathbf{x})/\gamma(\mathbf{x}), \quad \mathbf{x} \in \Gamma. \tag{4}$$

The surface gravity disturbance δg compares the magnitudes of the actual gravity $g = |\nabla W|$ and normal gravity $\gamma = |\nabla U|$ at the same point \mathbf{x}

$$\delta g(\mathbf{x}) = g(\mathbf{x}) - \gamma(\mathbf{x}), \quad \mathbf{x} \in R^3. \tag{5}$$

Moreover, we assume that T is regular at infinity, i.e.,

$$T = O(|\mathbf{x}|^{-1}) \text{ as } \mathbf{x} \rightarrow \infty \tag{6}$$

Equations (2), (3) and (6) represent the exterior oblique derivative BVP for the Laplace equation, because the normal to the Earth's surface Γ does not coincide with the vector \mathbf{s} defined by Eq. (4). The oblique derivative BC in Eq. (3) contains an error that arises from a linearization of the general gravimetric BVP (cf. Bjerhammar and Svensson 1983; Grafarend 1989). Here the surface deflection of the vertical is neglected as well, because the direction of $\mathbf{g} = \nabla W$ does not correspond to the direction of \mathbf{s} .

3 The direct BEM formulation for the linearized FGBVP

The underlying objective in a derivation of BEM is to replace the PDE that governs the solution in a domain by an equation that gives the solution on the boundary only (see, e.g., Brebbia et al. 1984; Hartmann 1989; Schwarz et al. 1990; Lucquin and Pironneau 1998). There are two fundamental approaches to the derivation of an integral equation formulation of the Laplace equation. The first is often called the direct method and the integral equations can be derived through the application of Green's third identity. The second technique is called the indirect method, which is based on the assumption that harmonic functions can be expressed in terms of a single-layer or double-layer potential generated by continuous source density functions defined on the boundary.

A conceptual disadvantage of the indirect BEM formulation is the introduction of the formal source densities usually without a direct physical relation to the problem. This can be overcome by using the direct BEM formulation, where values of the function and its normal derivative over the boundary Γ play the role of the source densities in generating the harmonic function over the solution domain (Brebbia et al.

1984). The integral equations can be derived using Green's third identity, where a harmonic function is represented as a superposition of the single-layer and double-layer potential. The same integral relation can be obtained through the method of weighted residuals. Here we briefly outline its main principle.

Let us seek an approximate solution to the problem governed by the Laplace equation (2), with BC of the Dirichlet type

$$T(\mathbf{x}) = \bar{T}(\mathbf{x}), \quad \mathbf{x} \in \Gamma_1, \tag{7a}$$

or the Neumann type

$$\frac{\partial T}{\partial n_\Gamma}(\mathbf{x}) = \bar{q}(\mathbf{x}), \quad \mathbf{x} \in \Gamma_2, \tag{7b}$$

where \mathbf{n}_Γ is the normal to the boundary Γ . \bar{T} and \bar{q} are prescribed values of the function and its normal derivative over the boundary Γ . Notice that $\Gamma = \Gamma_1 \cup \Gamma_2$.

The error, introduced by replacing T and q by an approximate solution, can be minimized using the following weighted residual consideration:

$$\int_{\Omega} \Delta T(\mathbf{y})w(\mathbf{x}, \mathbf{y})d\mathbf{y} = \int_{\Gamma_1} [T(\mathbf{y}) - \bar{T}(\mathbf{y})] \frac{\partial w(\mathbf{x}, \mathbf{y})}{\partial n_\Gamma(\mathbf{y})} d\mathbf{y} - \int_{\Gamma_2} [\frac{\partial T}{\partial n_\Gamma}(\mathbf{y}) - \bar{q}(\mathbf{y})]w(\mathbf{x}, \mathbf{y})d\mathbf{y}, \tag{8}$$

$\mathbf{x} \in \Gamma,$

where w is a weighting function. A double integration by parts of the left-hand side of Eq. (8) yields

$$\int_{\Omega} \Delta T(\mathbf{y})w(\mathbf{x}, \mathbf{y})d\mathbf{y} = \int_{\Gamma_1} \frac{\partial T}{\partial n_\Gamma} w(\mathbf{x}, \mathbf{y})d\mathbf{y} + \int_{\Gamma_2} \bar{q}(\mathbf{y})w(\mathbf{x}, \mathbf{y})d\mathbf{y} - \int_{\Gamma_1} \bar{T}(\mathbf{y}) \frac{\partial w(\mathbf{x}, \mathbf{y})}{\partial n_\Gamma(\mathbf{y})} d\mathbf{y} - \int_{\Gamma_2} T(\mathbf{y}) \frac{\partial w(\mathbf{x}, \mathbf{y})}{\partial n_\Gamma(\mathbf{y})} d\mathbf{y} + \int_{\Omega} T(\mathbf{y})\Delta w(\mathbf{x}, \mathbf{y})d\mathbf{y}, \quad \mathbf{x} \in \Gamma. \tag{9}$$

Comparing the right-hand sides of Eq. (8) and Eq. (9), gives

$$\begin{aligned} & - \int_{\Omega} T(\mathbf{y}) \Delta w(\mathbf{x}, \mathbf{y}) d\mathbf{y} + \int_{\Gamma} T(\mathbf{y}) \frac{\partial w(\mathbf{x}, \mathbf{y})}{\partial n_{\Gamma}(\mathbf{y})} d\mathbf{y} \\ & = \int_{\Gamma} \frac{\partial T}{\partial n_{\Gamma}}(\mathbf{y}) w(\mathbf{x}, \mathbf{y}) d\mathbf{y}, \quad \mathbf{x} \in \Gamma. \end{aligned} \quad (10)$$

Now let the weighting function w be the fundamental solution of the Laplace equation, known as Green's function G ,

$$G(\mathbf{x}, \mathbf{y}) = \frac{1}{4\pi r}, \quad \mathbf{x}, \mathbf{y} \in R^3, \quad (11)$$

where $r = |\mathbf{x} - \mathbf{y}|$. Then its normal derivative with respect to the outward normal \mathbf{n}_{Γ} to the boundary at the point \mathbf{y} is

$$Q(\mathbf{x}, \mathbf{y}) = \frac{\partial G(\mathbf{x}, \mathbf{y})}{\partial n_{\Gamma}(\mathbf{y})} = \frac{\langle \mathbf{r}, \mathbf{n}_{\Gamma}(\mathbf{y}) \rangle}{4\pi r^3}, \quad \mathbf{x}, \mathbf{y} \in R^3. \quad (12)$$

Considering properties of the fundamental solution G in the first term of Eq. (10), it can be rewritten into the form (for more details see Brebbia et al. 1984)

$$\begin{aligned} & \frac{1}{2} T(\mathbf{x}) + \int_{\Gamma} T(\mathbf{y}) Q(\mathbf{x}, \mathbf{y}) d\mathbf{y} \\ & = \int_{\Gamma} \frac{\partial T}{\partial n_{\Gamma}}(\mathbf{y}) G(\mathbf{x}, \mathbf{y}) d\mathbf{y}, \quad \mathbf{x} \in \Gamma. \end{aligned} \quad (13)$$

The BIE in Eq. (13) represents the direct BEM formulation for the Laplace equation. An advantage is that the restriction for the boundary surface to be a Liapunov (smooth) one can be relaxed. In fact, Eq. (13) can be applied to the more general Kellogg regular surfaces allowing corners or edges (Brebbia et al. 1984) provided that it is considered in the form

$$\begin{aligned} & c(\mathbf{x}) T(\mathbf{x}) + \int_{\Gamma} T(\mathbf{y}) Q(\mathbf{x}, \mathbf{y}) d\mathbf{y} \\ & = \int_{\Gamma} \frac{\partial T}{\partial n_{\Gamma}}(\mathbf{y}) G(\mathbf{x}, \mathbf{y}) d\mathbf{y}, \quad \mathbf{x} \in \Gamma, \end{aligned} \quad (14)$$

with a coefficient c . There are two different procedures for evaluating the coefficient c ; (i) through physical considerations, which arise from the fact that a constant potential applied over a closed body produces no flux, and (ii) through geometrical considerations (see later). Let us note that the BIE in Eq. (14) can be directly applied to evaluate the harmonic function T in any points $\mathbf{x} \in R^3 - \Omega$. In this case, the coefficient c equals one.

In this paper, we apply the direct BEM formulation (Eq. 14) to the linearized FGBVP described in Sect. 2. According to the oblique derivative BC in Eq. (3), $\nabla T(\mathbf{x})$ projected to $\mathbf{s}(\mathbf{x})$ equals to $-\delta g(\mathbf{x})$. Neglecting the surface (Helmert) deflection of the vertical, the normal derivative term $\partial T / \partial n_{\Gamma}$ in Eq. (14) is approximately equal to $-\delta g(\mathbf{x}) \cos \mu(\mathbf{x})$, where $\mu(\mathbf{x})$ is the angle $\angle(\mathbf{n}_{\Gamma}(\mathbf{x}), \mathbf{s}(\mathbf{x}))$. Let us

note that this term represents the projection of the vector $\delta g(\mathbf{x}) \mathbf{s}(\mathbf{x})$ (not exactly of the vector $\nabla T(\mathbf{x})$) to the normal $\mathbf{n}_{\Gamma}(\mathbf{x})$. The error of such approach is proportional to the error already included in Eq. (3). In this way, the oblique derivative BC in Eq. (3) is incorporated into the direct BEM formulation Eq. (14). Another approach using generalized Green's theorem would be also possible, but we do not follow it in this paper.

3.1 Collocation with linear basis functions

In the proposed approach, a collocation method with linear basis functions (denoting the C^1 collocation) is used for deriving the linear system of equations from Eq. (14). The Earth's surface as a boundary of the domain is approximated by the triangulation of the topography – expressed as a set of panels $\Delta \Gamma_j$. The vertices x_i, \dots, x_N of the triangles represent the nodes – the collocation points.

The C^1 collocation involves approximating the boundary functions by a linear function on each triangular panel using linear basis functions (Brebbia et al. 1984), i.e.,

$$T(\mathbf{x}) \approx \sum_{k=1}^3 T_k \psi_k(\mathbf{x}), \quad \mathbf{x} \in \Delta \Gamma_j, \quad (15a)$$

$$\delta g(\mathbf{x}) \approx \sum_{k=1}^3 \delta g_k \psi_k(\mathbf{x}), \quad \mathbf{x} \in \Delta \Gamma_j, \quad (15b)$$

where T_k and δg_k for $k = 1, 2, 3$ represent values of the boundary functions at the vertices of the triangular panel $\Delta \Gamma_j$. The linear basis functions $\{\psi_1, \psi_2, \dots, \psi_N\}$ are given by

$$\psi_j(\mathbf{x}_i) = 1, \quad \mathbf{x}_i = \mathbf{x}_j, \quad (16a)$$

$$\psi_j(\mathbf{x}_i) = 0, \quad \mathbf{x}_i \neq \mathbf{x}_j, \quad (16b)$$

where $i = 1, \dots, N$; $j = 1, \dots, N$ and N is the number of the collocation points. These approximations allow to Eq. (14) to be reduced to a discrete form for each collocation point i

$$\begin{aligned} & c_i T_i \psi_i + \sum_{j=1}^N \int_{\text{supp} \psi_j} \frac{\partial G_{ij}}{\partial n_{\Gamma}} T_j \psi_j d\Gamma_j \\ & = \sum_{j=1}^N \int_{\text{supp} \psi_j} G_{ij} \delta g_j \psi_j d\Gamma_j, \quad i = 1, \dots, N, \end{aligned} \quad (17)$$

where $\text{supp} \psi_j$ is the support of the j th basis function.

The coefficient c_i in Eq. (17) represents a “spatial segment” bounded by the panels joined at the i th collocation point. In the case of the linear basis functions, it can be evaluated by (Balaš et al. 1985)

$$c_i = \sum_{s=1}^S \frac{\varphi_{i_s}}{4\pi} (1 - \cos \phi_{i_s}), \tag{18}$$

where φ_{i_s} is the angle between two planes intersecting in $\mathbf{n}_e(x_i)$ and creating two edges of the s th triangle of the $\text{supp}\psi_i$. ϕ_{i_s} is the angle between $\mathbf{n}_e(x_i)$ and the s th triangle. S represents the number of triangles in the $\text{supp}\psi_i$.

Equation (17) represents the system of equations that can be rewritten into the matrix–vector form

$$\mathbf{M}\mathbf{t} = \mathbf{L}\delta\mathbf{g}, \tag{19}$$

where $\mathbf{t} = (T_1, \dots, T_N)^T$ and $\delta\mathbf{g} = (\delta g_1, \dots, \delta g_N)^T$. Coefficients of the matrices \mathbf{M} and \mathbf{L} represent integrals that need to be computed using an appropriate discretization of the integral operators in Eq. (17). The discretization of the integral operators is affected by the weak singularity of the kernel functions. The integrals with regular integrands, which represent non-diagonal coefficients, are approximated by the Gaussian quadrature rules defined on a triangle (Laursen and Gellert 1978). Their discrete form is (Čunderlík et al. 2002)

$$L_{ij} = \frac{1}{4\pi} \sum_{s=1}^S A_{j_s} \cos \mu_{j_s} \sum_{k=1}^K \frac{1}{r_{ik_s}} \psi_k w_k, \quad i \neq j, \tag{20a}$$

$$M_{ij} = \frac{1}{4\pi} \sum_{s=1}^S A_{j_s} k_{ij_s} \sum_{k=1}^K \frac{1}{r_{ik_s}^3} \psi_k w_k, \quad i \neq j, \tag{20b}$$

where A_{j_s} is the area of the s th triangular element of the $\text{supp}\psi_j$, k_{ij_s} is the perpendicular from the collocation point i to this planar element, K is the number of points used for the Gaussian quadrature with their corresponding weights w_k and linear basis functions ψ_k , r_{ik_s} is the distance from the i th collocation point to the k th quadrature point of the s th triangular element and $\cos \mu_{j_s}$ represents a projection of s (defined by Eq. (4)) in the j th collocation point to the normal \mathbf{n}_F of the s th planar element. Then the j th component of the vector $\delta\mathbf{g}$ in Eq. (19) corresponds to the input value of the measured surface gravity disturbance δg at the j th collocation point.

The non-regular integrals (singular elements) arise only for the diagonal components of the linear system. They require special evaluation techniques in order to handle the singularity of the kernel function. Thanks to the diagonal component c_i and the orthogonality of the normal to its planar triangular element, we obtain (Balaš et al. 1985)

$$M_{ii} = c_i. \tag{21}$$

The kernel function G (Eq. 11) in the integrals on the right-hand side of Eq. (17) is weakly singular. The diagonal coefficients L_{ii} can be evaluated analytically. After some elementary calculations using the *Mathematica*® software

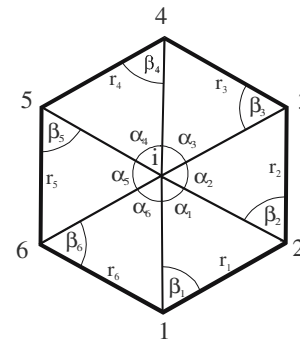


Fig. 1 Evaluating of the singular element (collocation with linear basis functions)

(Wolfram 1996), the analytical form is

$$L_{ii} = \frac{1}{2\pi} \sum_{s=1}^S \frac{A_{i_s}}{r_s} \ln \frac{tg[(\beta_s + \alpha_s)/2]}{tg(\beta_s/2)}, \tag{22}$$

where A_{i_s} is the area of the s th triangle of the $\text{supp}\psi_i$ determined by the line of length r_s and angles α_s , β_s (Fig. 1).

The diagonal component in Eq. (21) can be evaluated geometrically using Eq. (18) or through the physical consideration. The second approach is based on the fact that a constant potential applied over a closed body produces no flux. Accordingly, in case of the exterior Neumann problems, the sum of all components in each row should be equal to one (Brebbia et al. 1984). Then one can easily calculate coefficient c_i after evaluating of all non-diagonal coefficients of matrix \mathbf{M} using the Gaussian quadrature in Eq. (20b).

In Eq. (19), \mathbf{M} represents the stiffness matrix. Unfortunately, it is a nonsymmetric dense $N \times N$ matrix. However, the decay of the kernel function Q in Eq. (12) makes the stiffness matrix generally well conditioned. Consequently, non-stationary iterative methods can be efficiently applied to solve this large-scale linear system of equations. In our application the biconjugate gradient stabilized (BiCGSTAB) method (Barrett et al. 1994) is used, which is suitable for dense and nonsymmetrical matrices.

3.2 Gravity field modelling

An appropriate solution of the linear equation (19) provides the values of the unknown disturbing potential T at the collocation points directly on the Earth’s surface. Then one can easily evaluate the actual potential W or the geopotential numbers at the collocation points. In order to obtain a geometric quantity, the height anomaly ζ , the disturbing potential is rescaled using an expression analogous to the modified Bruns formula

$$\zeta(\mathbf{x}) \cong \frac{T(\mathbf{x})}{\gamma(\mathbf{x})}, \tag{23}$$

where $\gamma(\mathbf{x})$ is the magnitude of the normal gravity at the collocation point.

Here, there is an analogy with the Molodenskij problem (Molodenskij et al. 1962), which transforms the disturbing potential into height anomalies corresponding to the quasigeoid heights. Although the scaling factor γ in Eq. (23) is considered on the Earth's surface, in spite of the linearized Molodenskij problem where it is considered on a telluroid (Moritz 1980), we can identify $\zeta(\mathbf{x})$ with the quasigeoidal height. Therefore, we use the term quasigeoid for the disturbing potential rescaled by Eq. (23).

A superposition of the single-layer and double-layer potential in the direct BEM formulation (Eq. 14) allows us to use the mixed BC. In ocean areas, where mean sea surface (MSS) models are available from satellite altimetry, the Dirichlet BC can be defined. Then the same aforementioned functional model can be applied to the altimetry-gravimetry BVP. It only requires rearranging the system in Eq. (19) that yields a new stiffness matrix with different properties. In this way, unknown gravity disturbances can be obtained in areas of the oceans.

4 Efficient numerical solutions

Since the stiffness matrix \mathbf{M} is a dense and nonsymmetric $N \times N$ matrix, storage and time consumptions are of the order $O(N^2)$. In the presented numerical experiments, N is more than 10^5 . In order to solve such large-scale linear systems, computing on parallel computers, eventually clusters, is practically inevitable. In our approach, we use the standard MPI (message passing interface) subroutines for code parallelization (Aoyama and Nakano 1999). Here, the point-to-point and collective communication subroutines are implemented for the matrix assembly as well as for the BiCGSTAB linear solver.

Since every matrix component is independent of the others (each component M_{ij} represents a contribution of the j th element to the i th collocation point) and BiCGSTAB involves two matrix-vector products for each iteration (Barrett et al. 1994), the stiffness matrix \mathbf{M} can be parallelized to processors by the row-wise block distributions. Then only the known vector on the right-hand side of Eq. (19) and two residual vectors in BiCGSTAB need to be communicated between the processors. In this way, the time spent for communications between processors is minimized.

Numerous compression techniques developed in the last two decades can efficiently reduce the numerical complexity of the BEM. Here we briefly mention the fast multipole method, which approximates the kernel function in Eq. (11) factorizing the \mathbf{x}, \mathbf{y} dependency by a multipole expansion (Greengard and Rokhlin 1987). Hence, interactions of the far zones can be evaluated straightforwardly and the original

dense stiffness matrix \mathbf{M} is transformed into a sparse one. It can rapidly reduce the memory as well as the CPU-time consumption. An implementation of the fast multipole method as well as the panel clustering to the gravity field modelling by the Galerkin BEM is in Klees et al. (2001).

In our functional model, we have not yet implemented the fast multipole method. Instead, we use an approach that simply incorporates a priori known global solutions obtained: (i) from GGMs, where the low-frequency components are obtained from satellite missions, or (ii) from our numerical results computed on coarser grids without any far zone elimination. Considering the decay of the kernel function Q in Eq. (12), such approximate values of the disturbing potential are sufficient to evaluate a contribution of the far zones to any collocation point without a significant loss of accuracy. Consequently, all the “far zone components” of the original system matrix multiplied by the approximate values of the unknown disturbing potential will pass to the known vector on the right-hand side in Eq. (19). Then the original dense stiffness matrix is transformed into the sparse one, which becomes significantly better conditioned.

This approach reduces the memory requirements rapidly, while the CPU time-consumption remains almost unchanged. However, both integrations over the Earth's surface that determine coefficients of \mathbf{M} and \mathbf{L} in Eq. (19) are unchanged. It has at least two advantages: (i) errors that arise for the approximation of the kernel functions by the multipole expansion (Greengard and Rokhlin 1987), although very small, are not involved; (ii) the essential coefficient c_i derived through the physical consideration (see Sect. 3.1) can be evaluated more precisely. The price to be paid is the high CPU time-consumption. It can partly be reduced by decreasing an order of the Gaussian quadrature for ‘far zones’ elements with a minimum loss of accuracy (Sect. 5.1, Table 2). Nevertheless, implementation of the fast multipole method to our functional model could significantly improve the efficiency of the proposed approach.

5 Numerical experiments

The main objective of the numerical experiments is to demonstrate that the proposed approach of BEM applied to the linearized FGBVP gives the numerical solution of the Laplace equation (Eq. 2) directly on the real Earth's surface. The oblique derivative BC in the form of the surface gravity disturbances can be obtained from terrestrial gravimetry with precise satellite positioning and without demanding leveling. At the same time, the Earth's surface as the fixed boundary is prescribed. All these aspects are fundamental for the proposed approach.

The surface gravity disturbances as input data to our experiments are more or less simulated. This is because terrestrial

gravimetric measurements have been and are still followed by the precise levelling. However, precise 3D positioning by GNSS used in some modern gravimetry (cf. Kirby 2003) will eventually yield globally homogenous surface gravity disturbances.

The presented numerical experiments deal with both global and local gravity field modelling. In our effort, we focus on increasing accuracy of numerical solutions by refining a global triangulation of the Earth's surface as well as by local refinements. In order to extend numerical experiments, we reduce the enormous memory requirements in the way described in Sect. 4.2.

5.1 Global gravity field modelling

The first part of numerical experiments deals with global gravity field modelling. Unfortunately, we do not have at our disposal any database of the homogeneous input gravity data all over the Earth. Therefore, we use a GGM to simulate necessary input gravity disturbances. Consequently, our numerical results should converge to the corresponding GGM. This would confirm mathematical reliability of the numerical solution.

An application of the C^1 collocation to the direct BEM formulation (Sect. 3.1) involves a discretization of the boundary by a triangulation of the topography. First, we model the Earth's surface using the following datasets: (i) in continental areas, we add the SRTM30_PLUS V1.0 global topography model (Becker and Sandwell 2003) to EGM96 (Lemoine et al. 1998) in order to get geocentric positions, (ii) in ocean areas, we use the KMS04 MSS model (Andersen et al. 2005) transformed to the World Geodetic System 1984 (WGS84) (NIMA 2001) in the tide-free system.

Then, we approximate the above Earth's topography by a triangulated surface generated in the following way. We construct a triangulation using subdivisions of faces of a "12-hedron" (Fig. 2a). In every subdivision step, each triangle is divided into four congruent sub-triangles by halving the sides until a required level is reached (Fig. 2b). Such an algorithm generates horizontal positions, while the vertical coordinates, i.e., geodetic (ellipsoidal) heights, are

interpolated from the datasets described above. The vertices of the final triangulated surface represent the collocation points. The surface gravity disturbances at the collocation points are generated from EGM96 using the FORTRAN program GEOPOT97.V0.4.F (developed by Dru Smith, US National Geodetic Survey, in 2006). The parameters of the normal gravity field are given by WGS84.

Thanks to an opportunity to access high-performance computing (HPC) facilities (see the acknowledgments), the final large-scale computations were accomplished on the IBM SP5 high-speed parallel computer with 512 processors (about 1.2TB of distributed internal memory) at the CINECA HPC Centre. The standard MPI subroutines have been implemented for the code parallelization (Sect. 4.1). Particular numerical solutions for different levels of the global refinement are compared with EGM96. Basic statistical characteristics for the corresponding residuals as well as main computational aspects are shown in Table 1. A surface layout of the residuals on the reference ellipsoid for the largest experiment without any far zones elimination (124,418 collocation points) is depicted in Fig. 3.

The next part of the numerical experiments deals with a reduction of the enormous memory requirements. The developed algorithm eliminates interactions of the far zones by incorporating approximate values of the disturbing potential (Sect. 4.2) obtained from; (i) EGM96, or (ii) the numerical solution corresponding to the last column in Table 1. Such an approach rapidly reduces the memory requirements (Table 2). Consequently, a number of processors necessary for the same level of discretization can be reduced as the limit for the far zones decreases. This allows us to extend computations and to increase a level of the discretization considerably (Tables 2, 3; Fig. 4).

The particular refined numerical solutions are compared with EGM96. The basic statistical characteristics of the corresponding residuals are depicted according to the source of approximate values; (i) in Table 2 using the GGM, and (ii) in Table 3 for the second case. Table 2 shows the additional computational details as well. An influence of the chosen limit of far zones to accuracy of the numerical solution can be deduced from Table 2. The first five columns treat the

Fig. 2 Discretization of the Earth's surface; **a** subdivision of triangular faces of the "12-hedron" **b** the global triangulation of the topography

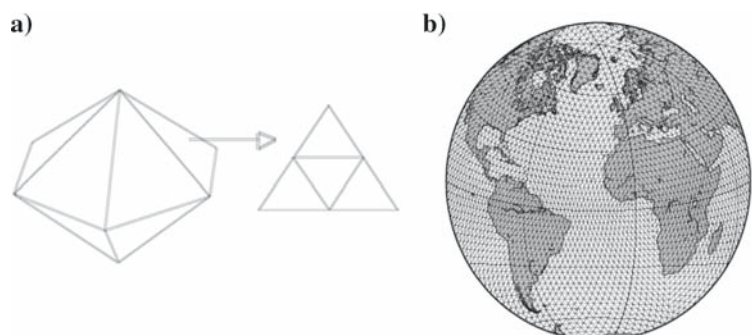


Table 1 Statistical characteristics of residuals between the numerical solution and EGM96 and corresponding computational aspects

N	44 378	48 602	60 002	124 418
$\Delta\phi$ (size of elements)	1.047°	1°	0.9°	0.625°
Residuals (BEM - EGM96)				
Mean				
Total	- 0.025 m	- 0.373 m	- 0.258 m	- 0.341 m
Oceans	-0.061 m	-0.302 m	-0.199 m	-0.275 m
Lands	+0.023 m	-0.515 m	-0.373 m	-0.509 m
Max				
Total	6.163 m	4.611 m	2.869 m	1.505 m
Oceans	4.156 m	3.754 m	2.869 m	1.505 m
Lands	6.163 m	4.611 m	1.981 m	0.602 m
Min				
Total	- 6.283 m	- 5.480 m	- 4.062 m	- 3.285 m
Oceans	-4.371 m	-3.770 m	-2.089 m	-2.019 m
Lands	-6.283 m	-5.480 m	-4.062 m	-3.285 m
SD				
Total	0.724 m	0.583 m	0.293 m	0.203 m
Oceans	0.520 m	0.485 m	0.230 m	0.151 m
Lands	0.937 m	0.729 m	0.376 m	0.306 m
Computational aspects				
Code	Serial	MPI	MPI	MPI
Memory requirements	15 GB	18 GB	28 GB	116 GB
Processors	1	12	16	80
Iterations	16	16	10	12
Matrix assembly	17 385 s	1 563 s	1 731 s	1 375 s
BiCGSTAB time	124 s	181 s	119 s	116 s
CPU time/procs	17 512 s	1 748 s	1 852 s	1 496 s
Total CPU time	17 512 s	20 976 s	29 632 s	119 680 s

Fig. 3 Residuals between the numerical solution and EGM96 (unmodified algorithm with the dense stiffness matrix – 124,418 collocation points (Table 1))

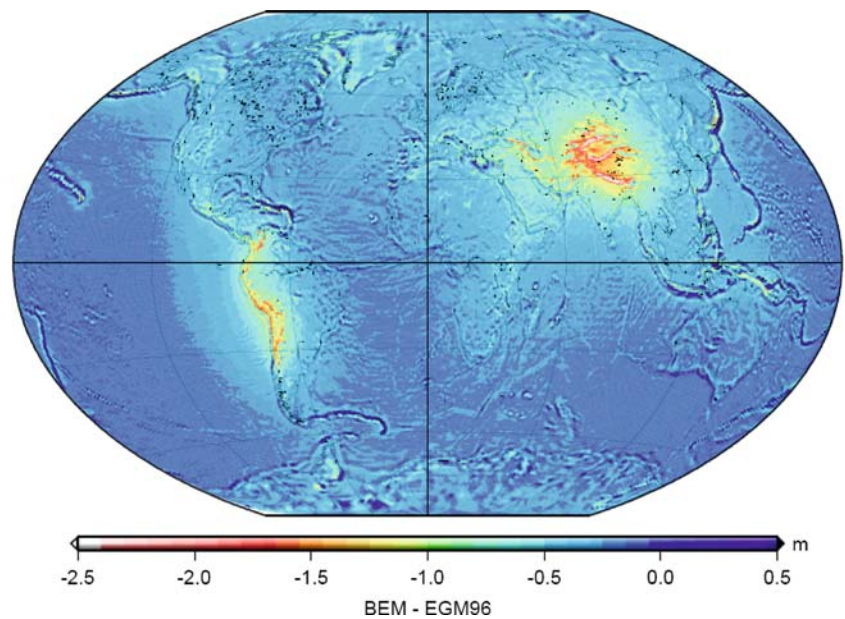


Table 2 Statistical characteristics of residuals between the refined numerical solution and EGM96 and reduction of memory requirements using the elimination of the far zones' interactions by incorporating EGM96 and corresponding computational aspects

N		124 418	124 418	124 418	124 418	124 418	194 402	375 002	1 215 002
$\Delta\phi$		0.625°	0.625°	0.625°	0.625°	0.625°	0.5°	0.36°	0.20°
Far zones	Limit	No	A/2	A/4	A/8	A/8	A/2	A/8	A/12
	Gauss q.	G7	G7	G7	G7	G3	G7	G3	G1
Residuals	Mean	- 0,341 m	- 0,457 m	- 0,508 m	- 0,538 m	- 0,539 m	- 0,507 m	- 0,614 m	- 0,632 m
	Max	1,505 m	1,248 m	1,195 m	1,164 m	1,163 m	0,727 m	0,268 m	-0,276 m
	Min	-3,285 m	-3,446 m	-3,525 m	-3,594 m	-3,603 m	-4,639 m	-2,657 m	-2,837 m
	SD	0,203 m	0,202 m	0,208 m	0,214 m	0,215 m	0,214 m	0,201 m	0,197 m
Memory requirements	Full <i>M</i>	116 GB	282 GB	1.05 TB	10.75 TB				
	Sparse <i>M</i>	116 GB	6.0 GB	1.43 GB	338 MB	338 MB	14.5 GB	3.25 GB	24.12 GB
Percentage of full matrix		100%	5.17%	1.24%	0.32%	0.32%	5.16%	0.31%	0.21%
Processors		80	8	10	10	10	22	24	42
Iterations		12	6	5	5	4	6	5	4
Matrix assembly		1 375 s	17 899 s	13 354 s	13 367 s	4 270 s	15 556 s	16 539 s	15 973 s
BiCGSTAB time		116 s	1997 s	9 s	4 s	5 s	38 s	16 s	14 s
CPU time/procs		1 496 s	19 901 s	13 369 s	13 375 s	4 281 s	15 602 s	16 573 s	16 037 s
Total CPU time		119 680 s	159 208 s	133 690 s	133 750 s	42 810 s	343 244 s	397 752 s	673 554 s

A semimajor axis of ellipsoid GRS-80, *G7* 7 Gaussian points (quadrature of the 5th order), *G3* 3 Gaussian points (linear quadrature), *G1* 1 Gaussian point (constant quadrature)

Table 3 Statistical characteristics of residuals between the refined numerical solutions and EGM96 and the elimination of the far zones interactions by incorporating the numerical solutions from the first column

N		124 418	194 402	375 002	1 215 002
$\Delta\phi$		0.625°	0.5°	0.36°	0.20°
Far zones	Limit	No	A/2	A/8	A/12
	Gauss q.	G7	G7	G3	G1
Residuals	Mean	-0,341 m	-0,343 m	- 0,347 m	-0,348 m
	Max	1,505 m	0,951 m	0,476 m	0,010 m
	Min	-3,285 m	-3,078 m	-2,541 m	-2,561 m
	SD	0,203 m	0,201 m	0,200 m	0,196 m

A semimajor axis of ellipsoid GRS-80, *G7* 7 Gaussian points (quadrature of the 5th order), *G3* 3 Gaussian points (linear quadrature), *G1* 1 Gaussian point (constant quadrature)

same discretization level, while the limit (denoted by the semi-major axis of the ellipsoid) is changing.

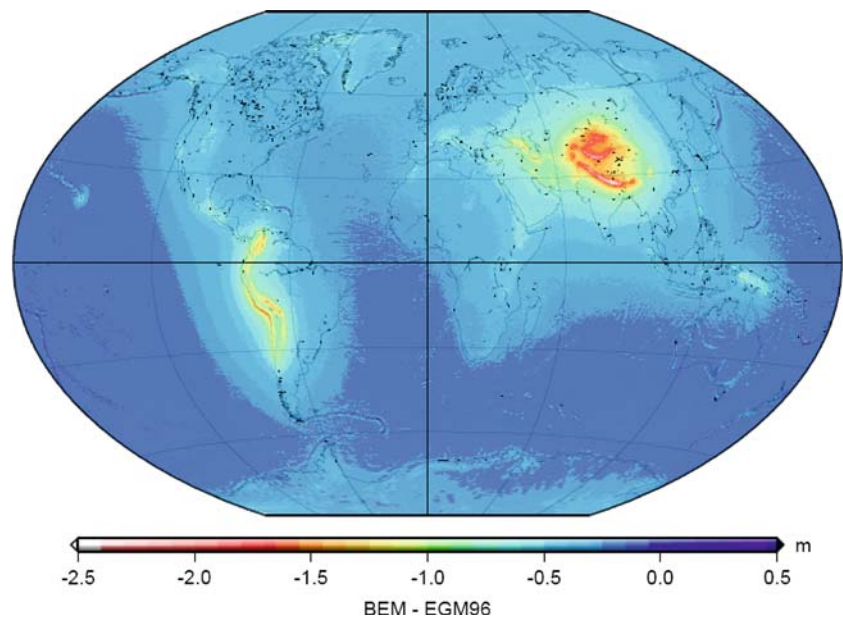
5.2 Local refinement for precise gravity field modelling

The proposed approach enables detailed gravity field modelling by a local refinement of the discretization. The computational procedure is the same as for the global treatment (Sect. 5.1). Small changes that arise from a local refinement of the global triangulation affect only “the list of neighbouring elements” (Čunderlík 2004). Similar to the global modelling, local gravity field modelling by BEM involves the integration over the whole Earth’s surface. The important difference is that a fine grid is used locally, while a coarse triangulation is used outside the refinement region

(Fig. 5). This reduces memory requirements and computational time. Moreover, the integration over the whole Earth’s surface brings an advantage that the local solution does not depend on GGMs in comparison with solutions based on the remove-restore technique.

The presented numerical experiment deals with the local solution in Slovakia, where we have at our disposal original gravity data. The local refinement of the triangulation is depicted in Fig. 5 (altogether 157,258 collocation points; 48,602 for the global triangulation and 108,656 for the local refinement). The smallest element represents a triangle of the area about 28'' × 40'' ($\Delta\phi \times \Delta\lambda$). As the available terrestrial gravimetric measurements have been accompanied by levelling (they have been collected for decades), we have to transform sea level heights to ellipsoidal (geodetic) heights.

Fig. 4 Residuals between the numerical solution and EGM96 (elimination of the far zones-the sparse stiffness matrix- 1,215,005 collocation points (Table 3))



Here we use the GMSQ03CF national quasigeoid model computed by the remove-restore technique and FFT-based methods (Mojzeš et al. 2005). We assume that the accuracy of GMSQ03CF is comparable with accuracy of levelling heights in lowlands, and slightly better in mountainous regions. In this way, we get the geocentric positions of the available gravimetric measurements. Note: this step vanishes in the case that the terrestrial gravimetry uses precise satellite positioning. Our input data set includes about 200 points of such data (cf. Kirby 2003) measured in extremely mountainous terrain in High Tatras, where precise levelling is practically impossible.

The input surface gravity disturbances at the collocation points are interpolated from values at points of discrete measurements. First, we transform the discrete surface gravity disturbances to complete Bouguer disturbances. Then, after gridding, we interpolate their values at the collocation points. Finally, we transform them back to the surface gravity disturbances at the collocation points using a digital terrain model comprising ellipsoidal heights. Here the most essential part is a precise evaluation of the topographical corrections at the discrete as well as the collocation points.

The final computations were accomplished on the IBM SP5 parallel computer. The performance, in terms of CPU-time, took 1083 s (about 18 min). The local (national) quasigeoid model in Slovakia as a numerical result of BEM applied to the linearized FGBVP is depicted in Fig. 6. Comparison with GPS/levelling indicates accuracy of the local numerical solution (Table 4, the case denoted by BEM). It shows an overall shift of the local solution about -18 cm. The standard deviation of 17 cm decreases to 6 cm after second-order polynomial fitting (6 coefficients). The residuals after fitting are depicted in Fig. 7a.

In order to compare our local solution with ones achieved by classical numerical techniques, we present the same GPS/levelling test for two other models (Table 4). Both of them are obtained by the remove-restore technique and FFT-based methods (Schwarz et al. 1990). The first represents a solution of the linearized FGBVP using the GRAVSOFT Package (Tscherning et al. 1994), while the Stokes kernel function is replaced by the Hotine (1969) kernel function inside the FORTRAN program SPFOUR. The second one is the GMSQ03CF national quasigeoid model (Mojzeš et al. 2005). It represents a solution of the linearized Molodenskij problem using the original SPFOUR program from GRAVSOFT. The residuals of the GPS/levelling test after second-order polynomial fitting for all three local quasigeoid models are depicted in Fig. 7.

6 Results and discussions

The numerical experiments of BEM applied to the linearized FGBVP apparently confirm the mathematical reliability of the proposed approach. The experiments dealing with the global quasigeoid modelling show that the achieved numerical solutions converge to EGM96 as the level of the discretization increases (Table 1). However, the achieved results represent numerical (approximate) solutions that include three different approximations (Lucquin and Pironneau 1998):

- The boundary is approximated by a piecewise polynomial surface defined by polynomials of degree t . In our case $t = 1$, i.e., the triangulation of the topography consists of planar panels.

Fig. 5 The local refinement of the triangulation in Slovakia

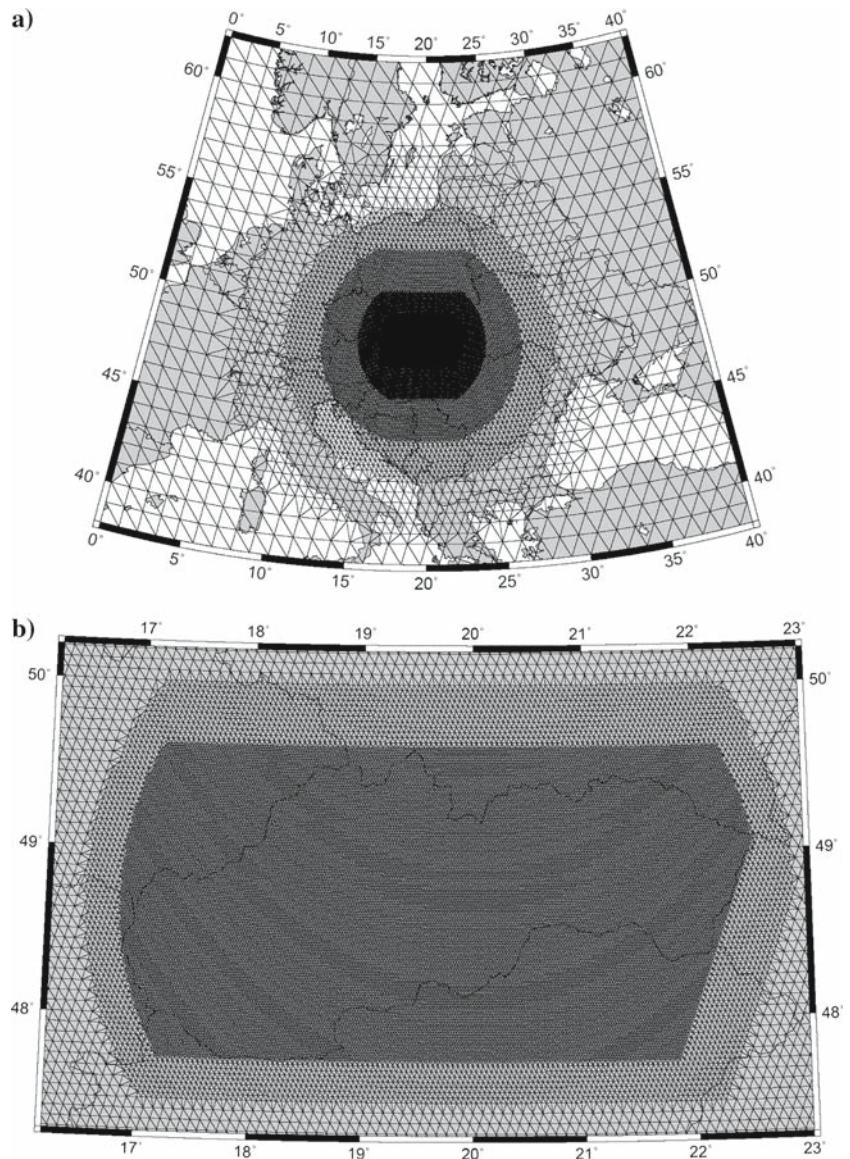


Fig. 6 The local (national) quasigeoid model in Slovakia (the local numerical solution of BEM applied to the linearized FGBVP)

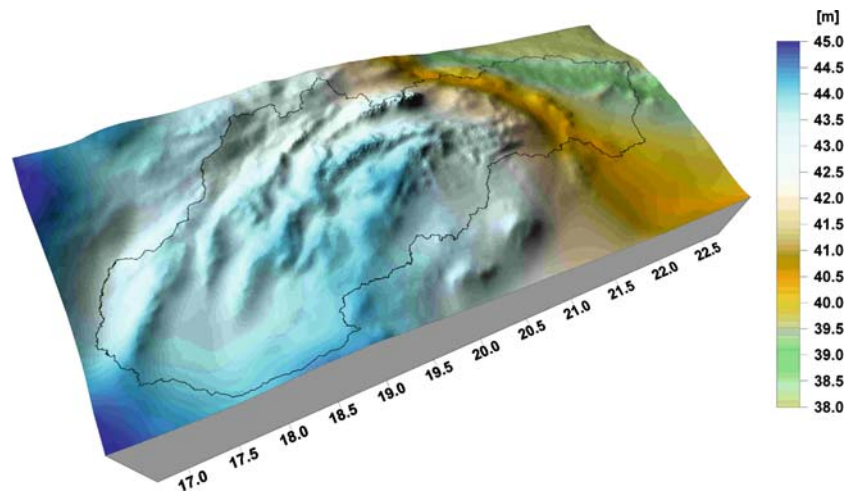


Table 4 GPS/levelling test for the local quasigeoid models - statistical characteristics of residuals before and after second-order polynomial fitting

BVP Method Resolution		The linearized FGBVP BEM 28'' × 40''		The linearized FGBVP FFT (gravsoft) 20'' × 30''		The lin. Molodenskij BVP FFT (gravsoft) 20'' × 30''	
Polynomial fitting		No	Yes	No	Yes	No	Yes
Coefficients		–	6	–	6	–	6
Test points		61	61	61	61	61	61
Residuals	Mean	−0.183 m	0.000 m	−0.385 m	0.000 m	−0.711 m	0.000 m
	Max	0.087 m	0.172 m	−0.226 m	0.098 m	−0.499 m	0.101 m
	Min	−0.624 m	−0.158 m	−0.523 m	−0.107 m	−0.875 m	−0.111 m
	SD	0.171 m	0.060 m	0.064 m	0.046 m	0.078 m	0.039 m

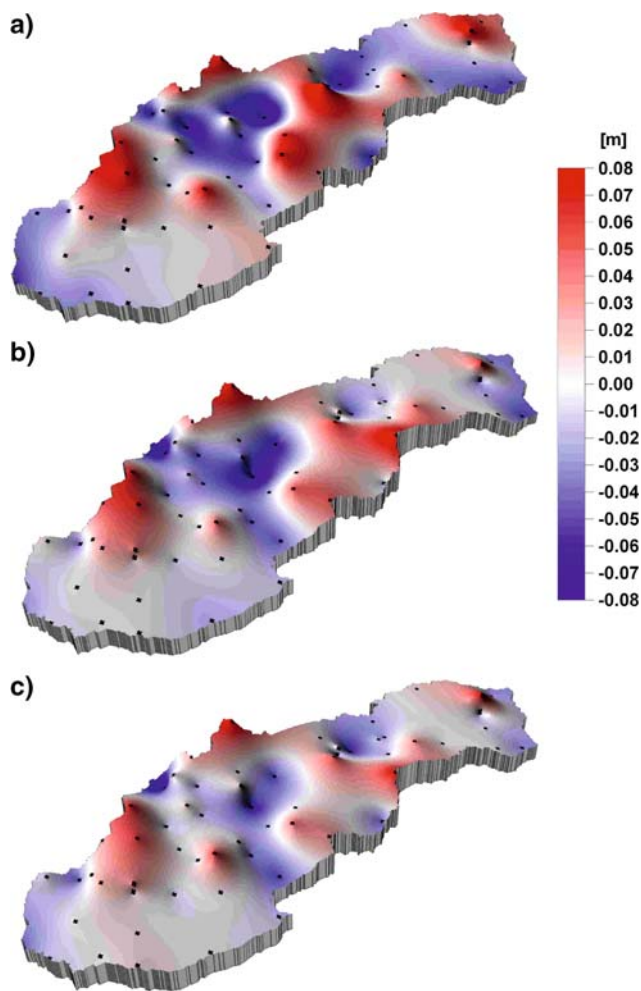


Fig. 7 GPS/levelling test residuals after second-order polynomial fitting (Table 4) from local quasigeoid models; **a** numerical solution of the linearized FGBVP by the proposed BEM approach, **b** solution of the linearized FGBVP by the remove-restore technique and FFT using the modified SPFOUR program from GRAVSOF, **c** GMSQ03CF - solution of the linearized Molodenskij problem by the remove-restore technique and FFT using the original SPFOUR program from GRAVSOF

- The boundary functions are approximated by piecewise polynomial functions of degree m . In our case $m = 1$, i.e., linear functions (the C^1 collocation) are used in Eq. (15).
- The Gaussian quadrature of the k th order is used for the discretization of integral operators in Eq. (19). In our case $k = 5$, i.e., seven Gaussian integration points are used.

Denoting the mesh size by r , the theoretical accuracy of the method is a function of all parameters r , t , m , k . There are some explicit expressions for the error estimation as a function of these parameters (Lucquin and Pironneau 1998). However, they require precision of the input boundary data, which is a problem in our case. Therefore we only mention that the applied method is approximately of the order $O(r^2)$. Consequently, instead of estimating the theoretical accuracy of the solution, we focus on the comparison of the numerical solutions with GGM, from which the input data are simulated.

The statistical characteristics of the residuals between the numerical solutions and EGM96 (Tables 1–3) confirm that a level of approximations decreases by refining the boundary's discretization. The standard deviation as well as maximal and minimal residuals decreases by refining the global triangulation. The mean values for 'unmodified' experiments (Table 1) are about -34 cm. It means that the achieved solutions are globally "smaller" than EGM96. It is due to a fact that the normal potential U_0 on the reference ellipsoid WGS-84 is smaller than an estimated value of the actual potential W_0 on the geoid (Lemoine et al. 1998).

Table 1 and Fig. 3 show that the numerical solutions better fit to EGM96 in areas of oceans and seas. There are evident residuals along boundaries of the lithospheric plates, e.g., in the Pacific Ocean (Fig. 3). It is probably due to an insufficient discretization along these zones, where the surface gravity disturbances abruptly change from extremely positive to extremely negative values. The maximal residuals are in the

Himalayas and Andes (Figs. 3, 4), especially on the edges of mountain ranges, where the quasigeoid is steeply undulating (zones of the highest deflection of the vertical). Here a small shift in the horizontal direction results in striking residuals in the vertical direction.

However, a quite nice agreement in the mountainous part of North America indicates that a more probable reason for the discrepancies in the Himalayas is due to a lack of terrestrial gravimetric measurements in this area. Another source of high residuals is that the sea level heights used to compute gravity anomalies and determined by levelling are subject to systematic errors and vertical datum offsets. This is probably the cause of large residuals in the mountainous parts of South America. With respect to gravity field modelling in mountainous areas, we reiterate that the proposed approach considers input data as well as the numerical solution on the real Earth's surface.

The next part of the numerical experiments focuses on a reduction of memory requirements. They demonstrate how to overcome this main drawback of the proposed approach. The elimination of the far zones' interactions by incorporating the a priori known coarse global solutions rapidly reduces the memory requirements (Table 2). This permits extension of the computations considerably by increasing a level of the discretization for the available number of processors. In this way, more precise solutions can be achieved (last columns in Tables 2, 3; Fig. 4).

Both unchanged integrations over the Earth's surface (matrices M and L in Eq. 19) keep their inner accuracy, but at the expense of the high CPU time. This explains why the standard deviations as well as the maximal and minimal residuals do not change much (cf. Table 2, first five columns). However, mean values change according to the source of approximate values of the disturbing potential.

- (i) When using EGM96, the mean values decrease consistently. The overall shift -34 cm from the previous "unmodified" experiments (Table 1) increases to -63 cm for the largest experiment (1,215,002 collocation points in Table 2). Here, the mean value in ocean areas is about -55 cm (standard deviation 9 cm). It corresponds to the adopted value of -54 cm of the correction to the height anomalies of EGM96 as a consequence of different values of U_0 and W_0 ; the zero-degree term (Lemoine et al. 1998).
- (ii) When using our numerical results computed on coarser grids (e.g., the largest experiment corresponding to the last column in Table 1), the mean values for higher resolutions go to -35 cm (Table 3) and to -28 cm in marine areas. The standard deviations are slightly better than those for the corresponding experiments in Table 2, e.g., 19.4 cm against 19.7 cm for the largest cases. Here we have to take into account that

a discrepancy between U_0 and W_0 is also involved in the input gravity disturbances. It can yield a 'double' effect included in the mean values for all experiments in the case (i).

Finally, the high CPU time consumption can be considerably reduced by decreasing the order of the Gaussian quadrature for evaluating the 'far zone elements' with a minimum loss of accuracy (compare the cases $A/8 + G7$ and $A/8 + G3$ for $N = 124, 418$ in Table 2).

The last numerical experiment shows that the proposed approach is also suitable for detailed quasigeoid modelling. It confirms that the local refinements provide more precise numerical solutions inside the refined areas. The GPS/levelling comparisons indicate precisions of all considered local quasigeoid models (see Sect. 5.2). The local numerical solution obtained by BEM is less precise (Table 4; Fig. 7) than models obtain by the remove-restore and FFT-based methods using GRAVSOF; compare the standard deviation 17.1 cm for BEM solution with 6.4 or 7.8 cm for FFT-solutions (Table 4).

The residuals after fitting (Fig. 7) show higher discrepancies at points in mountainous areas for all models. Here the inaccuracies of GPS and especially levelling are included. Residuals for the numerical solution by BEM (Fig. 7a) are more striking than the corresponding ones for the FFT-based models (Fig. 7b,c), (compare the maximal and minimal residuals before and after the polynomial fitting in Table 4). This, together with the high computational time and enormous memory requirements due to the integration over all Earth's surface, lowers the efficiency of the proposed approach in local quasigeoid modelling.

On the other hand, the BEM functional model allows a triangulation of the Earth's surface directly from the discrete terrestrial gravimetric measurements. Then all errors due to an interpolation of gravity data based on an evaluation of the topographical corrections (see Sect. 5.2) vanish. Consequently, a changed inhomogeneous configuration of the triangulation influences properties of the stiffness matrix and conditioning of the system in Eq. (19). An increase of the order of the Gaussian quadrature for nearest elements could give more precise local solutions.

Considering the computational aspects of all numerical experiments, the performance in terms of CPU time was always much longer for the matrix assembly than for the solution of the linear system (Tables 1, 2). The BiCGSTAB nonstationary iterative linear solver seems to be very efficient for all our numerical experiments. Thanks to well-conditioned stiffness matrix in the case of the pure oblique derivative BC (see Sect. 3.1), only several iterations of BiCGSTAB were necessary to keep an error lower than the prescribed tolerance ε in absolute residual error (Tables 1, 2). In all computations, $\varepsilon = 10^{-5}$ of the potential units ($\text{m}^2 \text{s}^{-2}$) and

we did not use any preconditioning. The elimination of the far zones interactions made the stiffness matrix even better conditioned. Corresponding elements were set to zero (the sparse stiffness matrix), while contributions of the far zones charged the known vector of the right-hand side of the system in Eq. (19). It affected the number of necessary iterations (compare Table 1 with Table 2).

We have tested the influence of the order of EGM96 geopotential coefficients used for elimination of the far zones' interactions to the accuracy of the numerical results. Thanks to the decay of the kernel function Q in Eq. (12), only the low frequency part ($n \approx 70$) was sufficient to get precise solutions. Only the overall bias due to a discrepancy between U_0 and W_0 affected mean values of the residuals between the numerical solutions and EGM96 (compare Tables 2 and 3). Of course, the aforementioned influence depends on a chosen limit for the far zones and on a level of the discretization.

7 Conclusion

The boundary element method (BEM) applied to the linearized fixed gravimetric BVP (FGBVP) provides a numerical solution directly on the Earth's surface. The direct BEM formulation using collocation with linear basis functions appears to be an efficient numerical tool for gravity field modelling. The oblique derivative boundary condition in the form of surface gravity disturbances has a striking practical advantage as the terrestrial gravimetric measurements can be positioned by GNSS without demanding levelling. Neglecting the deflection of the vertical leads to a possibility to use normal derivatives of the disturbing potential included in the direct BEM integral formulation, instead of the oblique derivatives.

The numerical experiments dealing with the global gravity field modelling apparently confirm the reliability of the proposed approach. A comparison with EGM96 shows that accuracy of the achieved numerical solutions increases by refining the discretization of the Earth's surface. The enormous memory requirements as a main limitation are rapidly reduced by the elimination of the far zones' interactions. Such an approach, as well as computing on parallel computers, enable to extend computations considerably and to get more precise numerical results. Precision of the obtained global quasigeoid models computed from simulated surface gravity disturbances is comparable with the precision of the GGM.

A local refinement in the area of original gravity data results in a reasonably precise local quasigeoid model. Although its precision is slightly worse than models obtained by classical approaches (e.g., remove-restore and FFT), such experiments indicate new opportunities for precise local gravity field modelling based on the adaptive refinement procedures. Their application, especially in zones of abrupt

changes of input data (both surface gravity disturbances and mountainous terrain), is a challenge for further investigations.

Acknowledgments The work has been performed under the Project HPC-EUROPA (RII3-CT-2003-506079), with the support of the European Community – Research Infrastructure Action under the FP6 “Structuring the European Research Area” Programme. Special thanks to the High Performance Centre CINECA (Consorzio Interuniversitario) in Bologna, Italy, namely to Giovanni Erbacci, Gerardo Ballabio and Fiorella Sgallari. The work has been partly supported by the grant VEGA 1/3321/06 and the project APVV-LPP-0216-06.

References

- Andersen OB, Knudsen P, Trimmer RG (2005) Improving high resolution altimetric gravity field mapping. In: Sanso F (ed) A window on the Future of geodesy, IAG symposia, vol 128, Springer, Berlin, pp 326–331
- Aoyama Y, Nakano J (1999) RS/6000 SP: Practical MPI programming. IBM, Poughkeepsie, New York
- Backus GE (1968) Application of a non-linear boundary-value problem for Laplace's equation to gravity and geomagnetic intensity surveys. *Q J Mech Appl Math* 2: 195–221
- Balaš J, Sládek J, Sládek V (1985) Analýza napětí metodou hraničných integrálních rovnic. Veda, Bratislava (in Czech)
- Barrett R, Berry M, Chan TF, Demmel J, Donato J, Dongarra J, Eijkhout V, Pozo R, Romine C, Van der Vorst H (1994) Templates for the solution of linearsystems: building blocks for iterative methods. <http://www.netlib.org/templates/Templates.html>.
- Becker J, Sandwell D (2003) Accuracy and resolution of Shuttle Radar topography mission data. *Geophys Res Lett* 30(9)
- Bjerhammar A, Svensson L (1983) On the geodetic boundary-value problem for a fixed boundary surface-satellite approach. *Bull Géod* 57:382–393
- Brebbia CA, Telles JCF, Wrobel LC (1984) Boundary element techniques, theory and applications in engineering. Springer, New York
- Čunderlík R (2004) Boundary element method applied to the Neumann geodetic boundary value problem. PhD Thesis, SvF STU, Bratislava
- Čunderlík R, Mikula K, Mojzeš M (2002) 3D BEM application to Neumann geodetic BVP using the collocation with linear basis functions. In: Proceedings of contributed papers and posters, ALGORITMY 2002, Conference on Scientific Computing, Vysoké Tatry-Podbanské, pp 268–275
- Čunderlík R, Mikula K, Mojzeš M (2004) A comparison of the variational solution to the Neumann geodetic boundary value problem with the geopotential model EGM-96. *Contr. to Geophysics & Geodesy*, vol 34, No. 3, Bratislava
- Grafarend EW (1989) The geoid and the gravimetric boundary-value problem. Rep 18 Dept Geod, The Royal Institute of Technology, Stockholm
- Greengard L, Rokhlin V (1987) A fast algorithm for particle simulation. *J Comp Physics* 73:325–348
- Hackbusch W, Nowak ZP (1989) On the fast matrix multiplication in the boundary element method by panel clustering. *Numerische Mathematik* 54:463–491
- Hartmann F (1989) Introduction to boundary elements. Theory and applications. Springer, Berlin
- Heck B (1989a) On the non-linear geodetic boundary value problem for a fixed boundary surface. *Bull Géod* 63:57–67
- Heck B (1989b) A contribution to the scalar free boundary value problem of physical geodesy. *Man Geod* 14:87–99

- Holota P (1997) Coerciveness of the linear gravimetric boundary-value problem and a geometrical interpretation. *J Geodesy* 71(10):640–651
- Holota P (2005) Neumann's boundary-value problem in studies on Earth gravity field: weak solution. In: 50 years of the Research Institute of Geodesy, Topography and Cartography, Prague, vol 50, 34:49–69
- Hörmander L (1976) The boundary problems of physical geodesy. *Arch Rat Mech Anal* 62:1–52
- Kirby JF (2003) On the combination of gravity anomalies and gravity disturbances for geoid determination in Western Australia. *J Geodesy* 77(7–8):433–439
- Klees R (1992) Lösung des fixen geodaetischen Randwertproblems mit Hilfe der Randelementmethode. DGK, Reihe C, Nr. 382, Muenchen
- Klees R (1998) Topics on boundary element methods. In: Sanso F, Rummel R (eds) geodetic boundary value problems in view of the one centimeter geoid. *Lecture Notes in Earth Sciences* vol 65, Springer, Heidelberg, pp 482–531
- Klees R, Van Gelderen M, Lage C, Schwab C (2001) Fast numerical solution of the linearized Molodensky problem. *J Geod* 75:349–362
- Koch KR, Pope AJ (1972) Uniqueness and existence for the geodetic boundary value problem using the known surface of the earth. *Bull Géod* 46:467–476
- Laursen ME, Gellert M (1978) Some criteria for numerically integrated matrices and quadrature formulas for triangles. *Int J Numer Methods Eng* 12:67–76
- Lemoine FG, Kenyon SC, Factor JK, Trimmer RG, Pavlis NK, Chinn DS, Cox CM, Klosko SM, Luthcke SB, Torrence MH, Wang YM, Williamson RG, Pavlis EC, Rapp RH, Olson TR (1998) EGM-96 - The Development of the NASA GSFC and NIMA Joint Geopotential Model. NASA Technical Report TP-1998–206861
- Lehmann R (1997a) Fast space-domain evaluation of geodetic surface integrals. *J Geod* 71:533–540
- Lehmann R (1997b) Solving geodetic boundary value problems with parallel computers. In: Sanso F, Rummel R (eds) Geodetic boundary value problems in view of the one centimeter Geoid. *Lecture Notes in Earth Sciences*, vol 65, Springer, Berlin
- Lehmann R (1997c) Studies on the use of boundary element methods in physical Geodesy. Publ. German Geodetic Commission, Series A, No. 113. Munich
- Lehmann R, Klees R (1996) Parallel setup of Galerkin equation system for a geodetic boundary value problem. In: Hackbusch W, Wittum G (eds) Boundary elements: implementation and analysis of advanced algorithms, Notes on Numerical Fluid Mechanics vol 54, Vieweg Verlag, Braunschweig
- Lucquin B, Pironneau O (1998) Introduction to scientific computing. Wiley, Chichester
- Molodenskij MS, Jeremejev BF, Jurkina MI (1962) Methods for study of the external gravitational field and figure of the Earth. Israel program for scientific translations, Jerusalem (translated from Russian original, Moscow, 1960)
- Mojzeš M, Janák J, Papčo J (2005) Gravimetric model of Quasigeoid in the area of Slovakia. *Acta Montanistica Slovaca* 10(2):161–165
- Moritz H (1980) Advanced physical Geodesy. Helbert Wichmann Verlag, Karlsruhe
- NIMA (2001) Department of Defense World Geodetic System 1984, Its definition and relationships With local Geodetic systems, 3rd edn, National Geospatial-Intelligence Agency. Technical Report TR8350.2
- Sacerdote F, Sansó F (1989) On the analysis of the fixed-boundary gravimetric boundary-value problem. In: Sacerdote F, Sansó F (eds) Proceedings of the 2nd Hotine-Marussi Symp Math Geod, Pisa, 1989, Politecnico di Milano, pp 507–516
- Schatz AH, Thomée V, Wendland WL (1990) Mathematical theory of finite and boundary element methods. Birkhäuser Verlag, Basel-Boston-Berlin
- Schwarz KP, Sideris MG, Forsberg R (1990) The use of FFT in physical geodesy. *Geophys J Int* 100(3):485–514
- Tscherning CC, Knudsen P, Forsberg R (1994) Description of the GRAVSOFTE package. Geophysical Institute, University of Copenhagen, Technical Report, 4th edn
- Wolfram S (1996) The Mathematica book. 3rd edn. Wolfram Media, Cambridge University Press, Cambridge